NASA Technical Memorandum 107042

Instantaneous Flow Measurements in a Supersonic Wind Tunnel Using Spectrally Resolved Rayleigh Scattering

Richard G. Seasholtz, Alvin E. Buggele, and Mark F. Reeder
Lewis Research Center
Cleveland, Ohio

Prepared for the
International Symposium on Optical Science, Engineering, and Instrumentation
sponsored by the Society of Photo-Optical Instrumentation Engineers
San Diego, California, July 9–14, 1995

National Aeronautics and
Space Administration

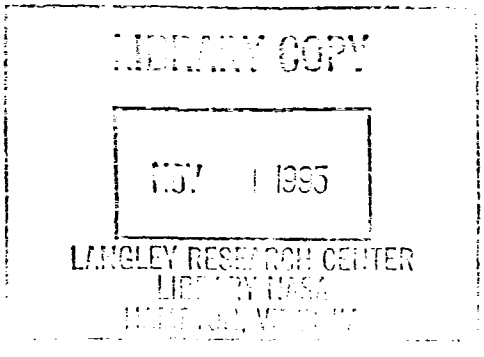

Instantaneous flow measurements in a supersonic wind tunnel using spectrally resolved Rayleigh scattering

Richard G. Seasholtz, Alvin E. Buggele, and Mark F. Reeder

NASA Lewis Research Center
Cleveland, Ohio 44135

ABSTRACT

Results of a feasibility study to apply laser Rayleigh scattering to non-intrusively measure flow properties in a small supersonic wind tunnel are presented. The technique uses an injection seeded, frequency doubled Nd:YAG laser tuned to an absorption band of iodine. The molecular Rayleigh scattered light is filtered with an iodine cell to block light at the laser frequency. The Doppler-shifted Rayleigh scattered light that passes through the iodine cell is analyzed with a planar mirror Fabry-Perot interferometer used in a static imaging mode. An intensified CCD camera is used to record the images. The images are analyzed at several subregions, where the flow velocity is determined. Each image is obtained with a single laser pulse, giving instantaneous measurements.

1. INTRODUCTION

Quantitative techniques for measurement of fluid flow properties in aerospace test facilities are needed to obtain performance data, to validate new computer codes, and to establish facility flow conditions. In many experiments, conventional probe measurements are not adequate because they perturb the flow under study. This is a particularly severe problem in high speed flows in small wind tunnels and in other confined flows such as occur in aircraft engine components. Instantaneous measurements are often needed in dynamic flow studies. It is also desirable in some experiments to obtain simultaneous measurements at a number of locations in the flow.

This paper presents the results of an experimental feasibility study to use laser Rayleigh scattering in a small supersonic wind tunnel to measure flow properties. Since Rayleigh scattering is a molecular scattering process, no seeding of the flow is needed. The Rayleigh scattering spectrum is directly related to the velocity distribution of the molecules; it therefore contains information about the thermodynamic parameters of the flow, including density, temperature and bulk velocity.

Because the frequency of the Rayleigh scattered light is at or near the frequency of the incident laser light, it is critical to control the stray laser light. In open flows such as free jets, it is relatively straightforward to prevent stray laser light from reaching the detection optics. The use of light traps, apertures, and baffles can greatly reduce detected stray light. In large flow facilities with open access these techniques can also be applied. One example is our previous Rayleigh scattering measurements for ASTVOL model tests in the Lewis 9 foot by 15 foot low speed wind tunnel[1]. On the other hand, in small flow facilities that usually require windows for optical access, it is generally difficult to control stray scattered light.

The Rayleigh scattering diagnostic described here is based on some of our previous Rayleigh scattering applications where a planar mirror Fabry-Perot interferometer was used in a static imaging mode (rather than a scanning mode) for one dimensional and planar temperature[2,3] and velocity measurements[4] in a free jet. We also made some previous measurements[5] in the tunnel used in the present study where the beam was introduced into the plenum and directed downstream through the test section. That arrangement, however, required removal of the flow conditioning at the nozzle entrance, which degraded the flow quality. In the present work, the laser beam is introduced into the tunnel near the second throat and is directed upstream through the test section. This arrangement permits use of the flow conditioners. However, a large amount of stray unshifted laser light is introduced into the field of view of the receiving optics. The Fabry-Perot does not have sufficient selectivity to reject this stray light while passing the Doppler-shifted Rayleigh scattered light. To overcome this problem, we added an iodine vapor absorption cell to prefilter the light reaching the Fabry-Perot. The collected light passes through the iodine cell, which blocks light at the laser frequency, and then is imaged through the Fabry-Perot interferometer onto an intensified CCD array detector. An important feature of the work presented here is that a

array detector. An important feature of the work presented here is that a single laser pulse is used to obtain measurements at number of localized regions in the flow, thus giving instantaneous measurements. If laser sheet illumination is used, measurements can be obtained at up to several hundred locations in one image[4], where the regions are located on the Fabry-Perot circular interference fringes. In the present work, however, the laser beam was focused to a line to achieve a higher single-to-noise with the single pulse, so measurements were obtained at only a small number of regions.

The use of the iodine absorption cell requires that the frequency of the Nd:YAG laser be known for each measurement. The approach used here is to use part of the CCD image to simultaneously record the Fabry-Perot fringe patterns of both unshifted YAG light and light from a frequency stabilized HeNe laser as well as the light collected from the tunnel which passes through the iodine cell. Analysis of the fringe patterns give the frequency of the YAG.

The results presented here were obtained in a recently modernized small subsonic/transonic/supersonic wind tunnel (SWT) having shock shape position control. The 3.81 in. by 10 in. (0.0968 m by 0.254 m) tunnel is a platform for evaluation testing intrusive and non-intrusive instrumentation systems and components on a continuing basis[6,7,8]. For this study, the tunnel was equipped with a Mach 2 nozzle. This SWT has many of the features of the larger tunnels at Lewis Research Center to adjust the boundary layers and thereby alter the normal shock trains and/or oblique shocks[9]. Shadowgraph flow visualization patterns were obtained at the the same flow conditions, although not on the same day.

The present effort is part of the non-intrusive instrumentation research and development program supporting supersonic and hypersonic propulsion research at Lewis. Optical techniques are under development to measure shock position for freestream flight Mach numbers of 1.5 to 4.5 or higher. Conventional wall static pressure taps are not expected to provide an accurate indication of shock position within a high speed inlet, partially due to the severe boundary layer problems expected during the operation of such an inlet. Large boundary layers in these inlets cause shock trains without well defined normal shock boundaries[10]. Oblique (reflective) shocks may also be present, further complicating the flow field.

The preliminary results presented in this paper demonstrate the feasibility of using Rayleigh scattering in high speed confined flows. The experimental results are limited to relatively low tunnel massflows because of various factors associated with flow induced vibrations in the optical system. Some intrusive instrumentation probe effects at Mach 2 are also present showing their disruptiveness.

2. THEORY

2.1 Molecular Rayleigh scattering

For a measurement volume illuminated by a laser pulse of energy E_o and wavelength λ, the number of detected photons collected by an optical system with solid collection angle Ω is (fig. 1)

$$N_R = \frac{\varepsilon E_o n L_x \lambda \Omega}{hc}\left(\frac{d\sigma}{d\Omega}\right)\sin^2\chi \qquad (1)$$

where ε is the overall collection efficiency (including the detector quantum efficiency), n the gas number density, L_x the length along the beam of the scattering volume, h Planck's constant, c the velocity of light, $d\sigma/d\Omega$ the differential scattering cross section, and χ the angle between the electric field vector of the (linearly polarized) incident light and the direction of the scattered light. For example, about 500 photons are collected by an f/8 optical system from a 1 mm^3 volume of nitrogen at NTP irradiated by a 1 mJ, 532 nm laser pulse.

The shape of the Rayleigh scattering spectrum is determined by the gas density and the optical configuration and is characterized by the nondimensional parameter $y = p/\eta Ka$, where p is the gas pressure, η is the shear viscosity, $K = (4\pi/\lambda)\sin(\theta_s/2)$ is the magnitude of the interaction wave vector $\mathbf{K} = \mathbf{k}_s - \mathbf{k}_o$ (with $\mathbf{k}_o$ and $\mathbf{k}_s$ being the wave vectors of the incident and scattered light), θ_s is the scattering angle, and $a = (2\kappa T/m)^{1/2}$ is the most probable molecular speed (with κ being Boltzmann's constant, m the molecular mass, T the gas temperature).

For low density gases and/or small scattering angles where $y<<1$, the normalized spectrum of the Rayleigh scattered light is given by the Gaussian

$$S(f)df = \frac{1}{\sqrt{\pi}\,aK}\exp\left\{-\left[\frac{2\pi(f-f_o)-\mathbf{K}\cdot\mathbf{u}}{aK}\right]^2\right\} \qquad (2)$$

where f_o is the laser frequency and $\mathbf{u}$ is the mean gas velocity. Note that the spectral peak is shifted by a frequency proportional to the component of the bulk velocity in the $\mathbf{K}$ direction. And the spectral width is proportional to the square root of the gas temperature.

For higher density gases (where the molecular mean free path becomes comparable to or smaller than the scattering interaction wavelength $2\pi/K$), the spectrum is no longer Gaussian in shape. For $y >> 1$ (high density gases), the scattering spectrum is strongly influenced by collective effects and is characterized by a central peak and two sidebands. The sidebands can be thought of as being caused by scattering from thermally excited acoustic waves. A continuum theory[11] can be used to model the spectrum here. The spectrum in the transition regime, where $y \sim 1$, requires a more detailed kinetic theory. We used the Tenti S6 model[12] for this work.

As, shown by equations 1 and 2, the Rayleigh scattered light collected from one vantage point contains sufficient information to determine the gas density, temperature, and one component of the bulk velocity. (Spectra measured at other $\mathbf{K}$ directions would give other velocity components). Density is proportional to the total Rayleigh scattering as given by equation 1. This generally requires a calibration to determine the proportionality constant. (Although it is also possible to determine the density from the spectral shape for a limited range of y parameters values[2,3].) Since typical molecular speeds are on the order of the speed of sound, the linewidth of the Rayleigh line is about 1 GHz for air and 90° scattering.

2.2 Spectral measurement methods

2.2.1 Absorption filters

Iodine vapor is the most commonly used filter medium because it has suitable absorption lines for both the 514.5 nm argon-ion laser and the 532 nm line of the frequency doubled Nd:YAG laser. Absorption filters are used in several techniques. One is to use a relatively slow cutoff edge of an absorption line, achieved using an optically thin filter (as in the Doppler Global Velocimeter[13]), or by pressure broadening the line by adding nitrogen to the absorption cell[14]. In this case, the filter acts as a frequency discriminator, where the transmitted light intensity is proportional to the frequency of the incident light. This technique is generally used with seeded flows, achieved with artificial seeding, or by using condensation formed in highly expanded flows.

The second technique is to use the very sharp transition between high absorption and transmission achieved with an optically thick filter, which blocks light at the laser frequency while passing light that is frequency shifted out of the absorption band. This Filtered Rayleigh Scattering technique[15] was developed to measure density, temperature, and velocity over a planar region. However, frequency scanning of the laser is generally needed to obtain temperature and velocity measurements, and thus the measurements are not instantaneous.

Another scheme, which is capable of instantaneous measurements, is the Angularly Resolved Filtered Rayleigh scattering technique[16], which utilizes the variation of the scattering spectrum with the $\mathbf{K}$ vector over the collection aperture. Although initially developed for point measurements, it can be extended to line measurements by using sheet illumination. A requirement in all the absorption filter techniques is accurate control of the laser frequency relative to the absorption line.

2.2.2 Fabry-Perot interferometers

The Fabry-Perot interferometer (as shown in fig. 2) consists of two partially transmitting planar mirrors. Multiple reflections between the mirrors result in a transmission function (defined as the fraction of light transmitted by Fabry-Perot for a monochromatic source) given by[17]

$$I_{FP}(f,\theta_r)=\left[1+F\sin^2\left(\frac{2\pi f\mu d_o\cos\theta_r}{c}\right)\right]^{-1} \tag{3}$$

Here, $f=c/\lambda_o$ is the optical frequency, μ is the refractive index of the medium in the Fabry-Perot cavity, d_o is the Fabry-Perot mirror spacing, θ_r is the angle between the ray and the optic axis, and $F = 1/(\sin^2(\pi/2N_E)$ where N_E is the effective finesse. The image of a monochromatic extended source located in the object plane consists of a series of concentric rings, such as shown in figure 3.

The Fabry-Perot interferometer has been used for analysis of Rayleigh scattering in both long range atmospheric measurements and in ground based flow test facilities. Used in a scanning mode, it gives a time average measurement of the spectrum at a point. Or, used in an imaging mode, it is capable of measuring the instantaneous spectrum of a single pulse. Another related technique, called the Edge Technique[18], uses the central fringe of a Fabry-Perot as a frequency discriminator.

The Fabry-Perot used in the static, imaging mode takes advantage of the angular sensitivity of the transmission to achieve frequency resolution. In this method a region of the flow illuminated with the laser light is imaged through the Fabry-Perot onto an array detector. As shown by equation 3, the fringe location is radially shifted by an amount related to the frequency shift of the scattered light The spectrum is only measured on the interference fringes and thus gives a spatial average over the part of the fringe being analyzed. However, with several fringes in the field of view, measurements can be obtained at a large number locations. This imaging method is the basis for the technique described in this paper.

A major difficulty occurs if a significant amount of stray laser light reaches the collecting optics. The Fabry-Perot interferometer used in a single pass mode with typical values of finesse does not have a high degree of selectivity. That is, a strong, single frequency source will dominate a weaker source even if its frequency is not close to the frequency of the strong source. The system described in this paper solves the problem of stray laser light by using an iodine absorption filter as a prefilter to the Fabry-Perot interferometer. The frequency of the 532 nm YAG line was set to be within an absorption line so light at the laser frequency is blocked while some or all of the frequency shifted Rayleigh scattered light is passed through to the Fabry-Perot.

2.2.3 Model of Rayleigh spectral measurements using Fabry-Perot and iodine absorption cell

Consider a laser beam of energy E_o that illuminates a region in the object plane. The expected number of detected photons for the q^{th} pixel (with area ΔA) can be written

$$<N_{Dq}>=\int_{\Omega}\int_{\Delta A}\int_{-\infty}^{\infty}[A_R S_R(f,\Omega)+A_W\delta(f-f_o)]I_{FP}(f,\theta_r)\,I_{I2}(f)\,df\,dA\,d\Omega+B_q \tag{4}$$

where A_R is the total amount of Rayleigh scattering that would be detected by the q^{th} pixel if the Fabry-Perot interferometer and iodine absorption cell were not present. Likewise, A_W represents the unshifted laser light scattered from windows and walls at the laser frequency $f_o=c/\lambda_o$. The spectrum of the Rayleigh scattered light is $S_R(f,\Omega)$, $I_{FP}(f,\theta_r)$ is the Fabry-Perot instrument function (eq. 3) and $I_{I2}(f)$ is the transmission function of the iodine cell. Broadband background light, detector dark current, and readout noise are represented by B_q. The integration over the solid angle is necessary to account for the range of **K** vectors over the light collection aperture. For small solid collection angles or low velocities, this effect can be neglected and the integration over Ω can be eliminated. The above model is for direct imaging onto the CCD array. However, for a camera with a microchannel plate intensifier, the effective spatial resolution is larger than a single pixel. For our camera, the point spread function (FWHM) is about two pixels. This is incorporated into the model function using a 2D fast Fourier transform to implement the convolution.

2.2.4 Filtered Rayleigh spectrum

The effect of an iodine absorption cell on the Rayleigh scattering spectrum is illustrated in figure 4. The iodine filter transmission was calculated using a code provided by J. Forkey[19,20]. The cell length is 200 mm, the iodine vapor pressure is 0.46 torr, and the cell temperature is 328 K. The scattering angle is 90°. For simplicity, the Gaussian form of the Rayleigh

spectrum was used. The flow is antiparallel to the incident laser beam, so the Rayleigh scattered light is shifted to higher frequencies relative to the laser frequency. For the f/3.6 collection aperture and relatively low velocities (~Mach 1.5), aperture broadening is minimal and has been neglected. (For the typical conditions in this work, aperture broadening causes an apparent increase in the temperature of less than 2 %.)

For a laser frequency close to the filter edge, with a sufficiently high Mach number flow, the Rayleigh scattered light is almost completely shifted out of the absorption band, and the spectrum is only slightly changed. In this situation, a least squares fit of the recorded image to the model given by equation 4 should give good estimates of both the mean velocity and the static temperature. However, if the laser frequency is not close to the filter edge or if the Mach number is relatively low (as was the case with the measurements described in this paper where the Mach number was ~ 1.5), the velocity and temperature parameters are not independent. In addition to the true fit, a reasonably good fit can also be obtained with a range of higher velocities and lower temperatures. For example, figure 4b shows the filtered spectrum for a higher velocity and lower temperature than shown in figure 4a (534 m/sec vs. 403 m/sec and 178 K vs. 200 K). The filtered spectra for these two cases are seen to be similar. The best situation is to have the laser frequency as close to the absorption band edge as possible while maintaining sufficient attenuation of light at the laser frequency (as shown in fig. 4c). In the work presented here we used an additional constraint by assuming that the flow was adiabatic, so the total temperature was conserved. This is a reasonable assumption since no appreciable heat exchange occurred downstream of the stagnation chamber. This fixed the static temperature for a given velocity and avoided the indeterminacy in the velocity and temperature parameters.

3. EXPERIMENT

3.1 Supersonic wind tunnel description

The modernized version of the nearly 50 year old facility provides ambient or heated, conditioned, filtered, continuous flow to a 3.81 in. x 10 in. test section nearly 8.0 feet long (fig. 5). The air supply to the tunnel was filtered to remove particulates with diameters larger than 0.2 μm. The inlet pressure could be varied up to a maximum of 35 psia. The tunnel exit pressure could be adjusted down to about 2 psia with mass flows less than 12 lbm/sec. Side walls are equipped to provide compartmentalized boundary layer bleed in the throat region of the Mach 2.0 nozzle blocks, while providing 12 in. by 47 in. optical access. Compartmentalized roof and floor modules immediately downstream of the nozzle blocks allow control of boundary layer thickness and/or angular adjustment of oblique shocks emanating from the nozzle exit. In addition, the figure reveals just a portion of the 50 throttle/adjustment valves for precise boundary layer bleed and/or injection control. Static pressure tap instrumentation exists every 0.5 inches midspan on these bleed modules. Likewise, numerous static taps exist in all other aluminum roof and floor segments of the SWT and/or its sidewalls. Also shown is the Mach 2.0 test rhombus, starting just forward of the 47 inch window near the three 1.5 (3.8 cm) inch diameter instrumentation ports (by the designated flow direction arrow). The instrumentation ports shown in the figure allowed the insertion of a 40° wedge probe or a dual total static probe into the developing or developed supersonic flow at 6.2 inches (0.15 m) forward of the nozzle exit on SWT centerline and/or 2.5 inches above/below SWT centerline. Also, about 8.0 inches (0.2 m) downstream of the nozzle exit is an insertible dual total-static probe to measure downstream Mach numbers of the developing test rhombus. The measured pressures are part of a 186 channel electronically sensed pressure system with an accuracy of ±0.033 psi (± 228 Pa). The Rayleigh scattering measurement region is about 2.0 in. (50 mm) downstream of the Mach 2.0 nozzle exit and 2.5 in. (64 mm) above the SWT floor. Optical access exists in the tunnel roof at the second throat for laser beam entrance.

3.2 Optical setup

The beam from an injection seeded, frequency doubled, Nd:YAG laser with 0.9 J pulse energy was focused with a pair of lenses (-200 mm and +200 mm focal lengths) into the wind tunnel through a window located in the top of the tunnel just forward of the second throat (figs. 5&6). A mirror located near the tunnel floor then reflected the beam upstream through the nozzle. The beam diameter at the measurement location was about 100 μm. A commercially available Fabry-Perot interferometer was used. The mirrors (70 mm diameter, λ/200 flatness, and 90% reflectivity) were set at a 14.96 mm spacing for the measurements reported here, which corresponded to free spectral range (FSR) of about 10 GHz. Rayleigh scattered light was collected at an 88.9° scattering angle through the tunnel sidewall window and collimated with lens L1 (250 mm focal length lens). The collimated light then passes through the iodine absorption cell (fused silica, 70 mm dia., 200 mm long). The cell has separate temperature controllers for the sidearm (to set the iodine vapor pressure) and for the cell body. After passing through the iodine cell, the light passes through an uncoated pellicle beamsplitter and the Fabry-Perot

interferometer. The light emerging from the Fabry-Perot was focused onto the detector (multichannel plate intensified, cooled CCD array with 576x384 23 μm square pixels) by lens L2 (300 mm focal length 35 mm camera lens with 1.4X teleconverter giving an effective focal length of 420 mm). This gives a field of view in the flow of 8.8 x 13.2 mm. The images were digitized with a 14 bit A/D converter and transferred to a laboratory computer for storage and analysis.

The following scheme was used to provide a YAG image of unshifted light and a measure of the absolute YAG frequency. The YAG image was needed to evaluate the Fabry-Perot interferometer phase and finesse for the unshifted light; the change between this phase and the phase of the Rayleigh scattered light is proportional to the velocity. A beamsplitter was used to direct a small amount of light from the YAG laser into an optical fiber; the fiber output was directed onto an opal glass diffuser. Light from a frequency stabilized helium-neon laser (633 nm, frequency stability equal ± 3 Mhz over 8 hr) was focused into a second optical fiber, and its output was directed onto the diffuser. A 135 mm camera lens collimated the light from the diffuser, which was directed into the Fabry-Perot via the pellicle beamsplitter. Note that this light did not pass through the iodine cell. Finally, a 0.76 mm diameter wire was placed in the focal plane of the 135 mm lens. This served to block unshifted YAG and HeNe laser light in the reference path from a horizontal strip in the CCD image; the blocked area comprised about 30 % of the total number of rows of pixels. The camera was operated in a gated mode with an exposure time of 0.08 sec. This enabled an adequate exposure of the HeNe light as well as light from a single YAG pulse. The test cell lights were turned off to limit ambient background light. Figure 8a shows a typical image with the Rayleigh scattered light (filtered through the iodine cell) in the central region and the YAG and HeNe reference light in the upper and lower parts of the image. Note that the HeNe fringes are wider than the YAG reference fringes because the interferometer finesse at 633 nm was less than the finesse at 532 nm. For this case the YAG frequency was 18788.456 cm^{-1}.

The entire optical setup (with the exception of the optics used to direct in the laser beam into the tunnel) was mounted on a aluminum optical breadboard, which was enclosed in a box covered with noise suppression material to minimize acoustically induced vibrations. Even though the acoustic noise level was reduced about 10 dB, the suppression was not adequate for all flow conditions as discussed below.

The frequency of the Nd:YAG laser was controlled with an analog voltage supplied to the injection seed laser. To determine the absolute YAG frequency, the input voltage to the injection seed laser was varied in discrete steps, with images of YAG light filtered by the iodine cell and the HeNe light recorded at each step. The two sets of fringes on each of the images were then analyzed to obtain the YAG frequency relative to the HeNe frequency over one Fabry-Perot order. An iodine absorption code supplied by J. Forkey was compared with the measured absorption spectrum to determine the absolute YAG frequencies. The 18788.45 cm^{-1} line was selected for this work because of the relatively sharp edge on the high frequency side, as well as its not having another close adjacent line on the high frequency side.

3.3 Experimental procedure

Because the Rayleigh Scattering Measurement System occupies the space adjacent to the SWT's test rhombus, simultaneous visualization of the flowfield was not possible. Flow conditions were usually established on a previous test day. Shadowgraph images were acquired with a NTSC, 646 x 486 pixel, black-and-white CCD camera. Most images were then enhanced, improving sharpness and brightness. Corresponding with flow visualization data all sensor and control data pressures, temperatures, valve settings, with specific parameters/calculations of Mach number, density, Reynolds number, mass flow rate, etc. are acquired by Lewis's Escort D central data acquisition system. Plenum pressure P7, static pressure P8 were measured 0.5 in. (1.3 cm) downstream of nozzle exit, Mach number Mn3 was located 8 in. (20 cm) downstream of the nozzle exit would be later precisely matched when taking the Rayleigh scattering data at a later time. The shadowgraph carriage was also positioned further downstream to view the Mn3 probe location. The Mn3 probe was usually limited to a 2.0 in. insertion into the aft portion of the rhombus so that test conditions would be easily duplicated. Refer to figure 5 for an isometric representation at maximum flow conditions. The intrusiveness of the Mn3 probe is minimized by its 0.25 in. by 0.125 in. diamond shape sting being only inserted 2.0 in. into the flow. A second pitot-static probe was positioned on the diamond-shaped sting, giving a Mach number well upstream of the Rayleigh scattering measurement volume. The Mach number was typically 1.8 when using this probe in the beginning portion of the test rhombus (fig. 7). These probes provided a means to compare the Rayleigh scattering data to a standard measurement approach. However, their locations far from the Rayleigh scattering measurement volume prevented a direct comparison.

After the flow condition was set, about ten images were taken, each with a single YAG pulse. The frequency of the YAG was adjusted to be close to the high frequency edge of the 18788.45 cm^{-1} iodine absorption line. The cold finger of the iodine cell was set to 30° C (vapor pressure = 0.46 T), and the cell body temperature was set to 55° C. The temperature of the stopcock on the iodine cell (which had the lowest temperature except for the iodine reservoir) was monitored to ensure that it remained higher than the cold finger temperature.

3.4 Data processing

The data reduction procedure was as follows. The first step was to analyze the upper and lower regions to determine both the Fabry-Perot interferometer phase and the frequency of the unshifted Nd:YAG light. (The measured finesse includes the effect of the finite linewidth of the Nd:YAG laser.) This was done by using a least-squares fit of the image to a model function that included both HeNe and YAG fringes. For example, figure 8b shows the locations of the first two fringes for both lasers for the image shown in figure 8a. A number of subregions in the recorded image were then defined on the fringes in the central horizontal strip. For this work we only used four subregions located on the inner two fringes (a typical set of subregions is shown in figure 8c). The image of the Rayleigh scattered light (filtered by the iodine cell) was analyzed using a nonlinear least-squares fit. The model function (eq. 4 plus a convolution of a 2D Gaussian function to account for the MCP image broadening) was evaluated at 9 points in each pixel for the numerical integration over the area of each pixel. A 50x50 pixel subregion (equal to about a 0.64 mm square) was used for the inner fringe, and a 35x35 pixel subregion (equal to about a 0.45 mm square) was used for the second fringe. The larger subregion size was needed for the inner fringe because the fringe width increases with decreasing fringe radii. As discussed above, the constraint of fixed total temperature was imposed. Therefore these results do not include an independent measurement of static temperature, as would be possible for higher Mach number flows. As a result of the extensive calculations required for the full evaluation of the model function for the iterative fitting procedure, the processing time is quite long—about 7 minutes on a 90 MHz Pentium PC for a 35x35 pixel subregion. The result of this procedure is a value for the velocity component and the gas temperature at each subregion. It should be noted that velocity and temperature data are only obtained for subregions located on the fringes; no data are obtained in the regions between fringes. To achieve more complete coverage, additional images can be obtained at different Fabry-Perot mirror spacings, which give fringes at different radii. (But then the data are not all obtained simultaneously.) In any case, the results obtained with this procedure for each subregion represent average values of velocity and temperature over the subregion. The flow direction was assumed to be along the tunnel axis for the purpose of converting the measured velocity component (which is along **K**) to the velocity magnitude. The y parameter was about 0.5, so the Tenti S6 model for the Rayleigh spectrum was used.

4. RESULTS

For the Rayleigh scattering data presented, an intrusive flow measurement was made using a 40° included angle wedge probe installed mid span on SWT centerline (see fig. 7). This probe was installed at the instrumentation port 6.2 in forward of the nozzle exit and indicated a Mach number of 1.95 - 2.04 for mass flows ranging between 11 to 28 lbm/sec. See visualization images 1323_1298 (13 lbm/sec) and 1326_1300 (16 lbm/sec) for typical low mass flow tunnel conditions where Rayleigh scattering data (located on bullseye) were obtained. The bow shock of the wedge probe interacts with the boundary layer to significantly disturb the flow and preclude the accurate measurement of the true flow conditions in this small area SWT. Deeper immersion into the flow creates a sting effect and creates a higher indicated Mach number than the true value. For example, the wedge probe indicated a 0.2 higher Mach number than the less intrusive dual static probe at these forward positions. The reference shadowgraph image 918 was taken at indicated Mach numbers of 1.78 at Mn2 and 1.43 at Mn3. Repositioning the 40° wedge probe 6.2 inches forward of the nozzle exit and 2.5 in. above the SWT centerline reveals the lower bow shock and the shock emanating from the wedge lower shoulder as well as a developed normal shock train, see figure 7 image 1315_1308 at 23 lbm/sec. No Rayleigh scattering data were obtained for this condition. The total temperature indicated just forward of the bow shock of the wedge probes measured 8.3 to 13.9 K higher than the static temperature measured via T8, which was installed (0.05 in. into boundary layer) inside the nozzle. The T8 measured temperature was used in all Mn3 density, massflow and Reynold's number calculations even though Mn3 was located 14 inches downstream of T8. Calculations of similar flow quantities from wedge probe data used temperature measurements obtained from the wedge probe. The non-centralized locations (upstream and downstream of the Rayleigh measurement station) of the temperature measurements introduced a significant amount of uncertainty in the computed flow conditions.

Results are shown for two flow conditions described in the table. The Rayleigh scattering measurements were made 50 mm downstream of the nozzle exit and 64 mm above the tunnel floor. The first, designated as RDG 1298, was at the same flow condition as shown in the shadowgraph (fig. 7, 1323_1298). The Rayleigh scattering measurement location for this case was just downstream of the apparent normal shock. The second condition, designated as RDG 1300 (shadowgraph 1326_1300 on fig. 7) , had the measurement region located just upstream of the shock. However, because the shadowgraphs were taken on a different day than the Rayleigh data, some uncertainty exists in the exact location of the shock train relative to the measurement volume. The velocities obtained for individual laser pulses are shown in figure 9 for the two flow conditions.

	RDG 1298	RDG 1300
Mass flow rate	13 lbm/sec	16 lbm/sec
Total temperature T7 (plenum)	296 K	296 K
Total pressure P7 (plenum)	16.9 psia	21.5 psia
Static pressure P8	6.28 psia	7.37 psia
Mach number MW (wedge probe)	1.95	1.95
Mach number MN3	0.94	1.00
mean axial velocity (std dev) -Rayleigh	414 (51) m/sec	445 (42) m/sec
mean temperature (std dev) -Rayleigh	209 (21) K	196 (18) K
mean Mach number (std dev) -Rayleigh	1.44 (0.26)	1.60 (0.22)

The table gives the flow parameter measurements obtained with conventional instrumentation and mean and standard deviations for the Rayleigh scattering results. The Rayleigh results are based on a total of 36 subregions for RDG 1298 and 34 subregions for RDG 1300. The average velocities were 414 and 445 m/sec for the two cases. These values are reasonable considering the flow visualizations in figure 7 and the pitot-static pressure data taken upstream and downstream of the Rayleigh scattering measurement location. As mentioned earlier, there is a fair degree of uncertainty associated with the exact locations of the shock train imaged in figure 7. The relatively large standard deviation in the instantaneous velocities are caused by flow variations and measurement errors. Assuming that the variation is due only to measurement error means that the Rayleigh velocity measurement uncertainty is about 10 %.

As discussed above, the temperatures shown are not based on an independent determination from the Rayleigh data, but are based on the assumption of adiabatic flow. The intensity of the Rayleigh scattered light was determined for each measurement, but the calibration needed to obtain an absolute density value was not done. Finally, figure 10 show the detected intensity of unshifted YAG light due to stray scattering in the tunnel filtered with the iodine cell as a function of the measured YAG frequency. These data include all the images obtained on one test day (not just the two sets used in fig. 9). As seen here, the YAG frequency ranged over both the absorbing and the transmitting portions of the spectrum, but the ideal frequency is just inside the cutoff frequency.

Several problems occurred in this study, which prevented obtaining Rayleigh data for all flow conditions . One problem was the high level of vibration of the tunnel itself, particularly at the higher mass flows. The resulting vibration of the beam directing mirror mounted on the tunnel floor caused the YAG beam direction to vary. The beam location in the image thus varied on a pulse-to-pulse basis. Another problem was the vibration of the Fabry-Perot interferometer, probably caused by the high acoustic noise levels in the test cell near the tunnel (about 103 dB). This resulted in an inability to adjust the Fabry-Perot to its maximum finesse for the high mass flows.

5. CONCLUDING REMARKS

Even using the least intrusively designed physical probes to measure supersonic flow in small/narrow supersonic wind tunnels can be highly disruptive. Any probe extended beyond the boundary layer affects the upstream and downstream flow field. However, for this study, use of intrusive probes were supportive as a crude means to establish the feasibility of the totally nonintrusive Rayleigh Scattering technique. Rather than a two-dimensional pass through diagnostic tool which only provides average data on velocity, direction, and/or temperature of the ever changing dynamic flowfield, Rayleigh scattering measurements can provide simultaneous, instantaneous measurements at a number of locations in the flow field.

Several conclusions may be drawn from this study. First is that a molecular absorption cell is a highly effective means to eliminate the effect of stray laser light, even for confined flows such as the supersonic wind tunnel used for this work. The intensity of the Rayleigh scattering was strong enough to enable measurements with a single laser pulse. Use of an absorption cell, however, means that the laser frequency must be controlled and accurately measured to enable correct modeling for processing the Rayleigh scattering data. The technique employed in this study for measuring the laser frequency (use of a frequency stabilized HeNe laser and Fabry-Perot interferometer) performed well, but required post

processing. A more direct measurement that gives an on-line readout of laser frequency, such as described in reference 19, would be preferable.

The use of the iodine absorption cell with the relatively low Mach numbers in this study required the assumption of adiabatic flow to avoid indeterminacy between the velocity and temperature in the data reduction. With high Mach number flows, the problem would not occur and velocity and temperature could be independently determined.

The test cell environment created a number of difficulties. Even though the optical system was located in an acoustic enclosure, the noise level at high mass flow caused intolerable vibration of the Fabry-Perot interferometer, and possibly of the Nd:YAG laser. Application of this technique must provide a stable environment for the vibration sensitive components including the laser and Fabry-Perot interferometer.

One feature not included in the present system that would enhance its usefulness would be remote control of the measurement region. Another very desirable addition would be automatic control of the Fabry-Perot alignment. The present procedure involves manual adjustment of the Fabry-Perot to maintain alignment, which takes time during the test and requires a skilled operator. Use of artificial neural nets may benefit this effort eventually. Finally, additional work needs to be done to provide on-line data reduction, with processing times on the order of a few seconds.

6. ACKNOWLEDGMENTS

We would like to acknowledge the efforts of Mr. W. Trevor John and Mr. Bertram Floyd, who were responsible for setting up and aligning the optical system used for this work, Mr. Salvatore Giordano, who was responsible for the wind tunnel preparation, and Mr. Kenneth Weiland, who was responsible for the shadowgraph system. Also, we thank Prof. G. Tenti for providing us with the computer code for his 6 moment Rayleigh scattering model, and Joseph Forkey for providing us with the iodine absorption code.

7. REFERENCES

1. H.E. Kourous and R.G. Seasholtz, "Fabry Perot interferometer measurement of static temperature and velocity for ASTOVL model tests", ASME Symposium on Laser Anemometry: Advances and Applications", Lake Tahoe, 1994.

2. J.L. Lock, R.G. Seasholtz, and W.T. John, "Rayleigh Brillouin scattering to determine one dimensional temperature and number density profiles of a gas flow field", Appl. Opt. **31**, pp. 2839- 2848, 1992.

3. R.G. Seasholtz and J.A. Lock, "Gas temperature and density measurements based on spectrally resolved Rayleigh-Brillouin scattering", NASA Langley Measurement Technology Conference, Hampton, VA, 1992.

4. R.G. Seasholtz, "2D velocity and temperature measurements in high speed flows based on spectrally resolved Rayleigh scattering", *New Trends in Instrumentation for Hypersonic Research*, A. Boutier (ed.), Kluwer Academic Publishers, Boston , 1993.

5. Seasholtz, R.G. "Instantaneous 2D velocity and temperature measurements in high speed flows based on spectrally resolved Rayleigh scattering", AIAA 33th Aerospace Sciences Meeting, Reno, AIAA paper 95-0300, 1995.

6. Boldman, D.R.; Buggele, A.E.; and Decker, A.J.: Three dimensional shock Structure in a transonic flutter cascade, AIAA Journal, Vol. 20, No. 8, pp 1146-1148, 1982.

7. Decker, A.J.; and Buggele, A.E.: Wind tunnel operations archival flow visualization records and artificial neural networks. AIAA 94-0390, 32nd Aerospace Sciences Meeting and Exhibit, Reno, NV, January 10-13, 1994.

8. Buggele, A.E.; and Decker, A.J.: Control of wind tunnel operations using neural net interpretation of flow visualization records. NASA Technical Memorandum 106683, for Ohio Area Neural Net Workshop sponsored by Ohio Aerospace Institute, Columbus, Ohio, August 16, 1994.

9. Shapiro, A.H., *The Dynamics and Thermodynamics of Compressible Fluid Flow*, New York: The Donald Press Company, Volume I, pages 135-142, 1953.

10. Shapiro, A.H., *The Dynamics and Thermodynamics of Compressible Fluid Flow*, New York: The Donald Press Company, Volume II, pages 1153-1159, 1954.

11. N.A.Clark, "Inelastic light scattering from density fluctuations in dilute gases. The kinetic hydrodynamic transition in monatomic gas", Phys. Rev. A **12**, 232- 244, 1975.

12. G. Tenti, C.D. Boley, and R.C. Desai, "On the kinetic model description of Rayleigh Brillouin scattering from molecular gases", Can. J. Phys. **52**, pp. 285-290, 1974.

13. J.F. Meyers and H. Komine, "Doppler Global Velocimetry: A new way to look at velocity", Laser Anemometry--Vol. 1, ASME, p. 289, 1991.

14. G.S. Elliott, M. Samimy, and S.A. Arnette, "Molecular filter-based diagnostics in high speed flows", AIAA 31th Aerospace Sciences Meeting, Reno, AIAA paper 93-0512, 1993.

15. R.B. Miles, W.R. Lempert, and J. Forkey, "Instantaneous velocity fields and background suppression by filtered Rayleigh scattering", AIAA 29th Aerospace Sciences Meeting, Reno, AIAA paper 91-0357, 1991.

16. J.A. Shirley and M. Winter, "Air mass flux measurement system using Doppler shifted filtered Rayleigh scattering", AIAA 31st Aerospace Sciences Meeting, Reno, AIAA paper 93-0513, 1993.

17. J.M. Vaughan, *The Fabry Perot Interferometer, History, Theory, Practice and Applications*, Adam Hilger, Bristol, Chapter 3, 1989.

18. C.L. Korb, B.M. Gentry, and C.Y. Weng, "Edge technique: theory and application to the lidar measurement of atmospheric wind", Appl. Opt. 31, pp. 4202-4213, 1992.

19. J.N. Forkey, N.D. Finkelstein, W.R. Lempert, and R.B. Miles, "Control of experimental uncertainties in filtered Rayleigh scattering measurements", AIAA 33th Aerospace Sciences Meeting, Reno, AIAA paper 95-0298, 1995.

20. R.B. Miles, J.N. Forkey, N. Finkelstein, and W.R. Lempert, "Precision whole-field velocity measurements with frequency-scanned filtered Rayleigh scattering", Proceedings of 7th International Symposium on Applications of Laser Techniques to Fluid Mechanics, Lisbon, 1994.

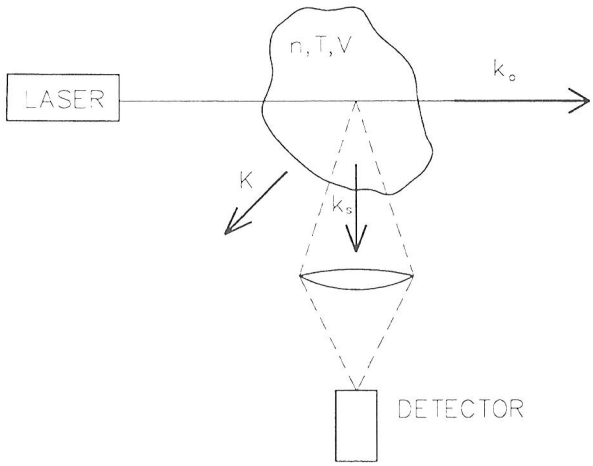

Figure 1.—Rayleigh scattering experiment.

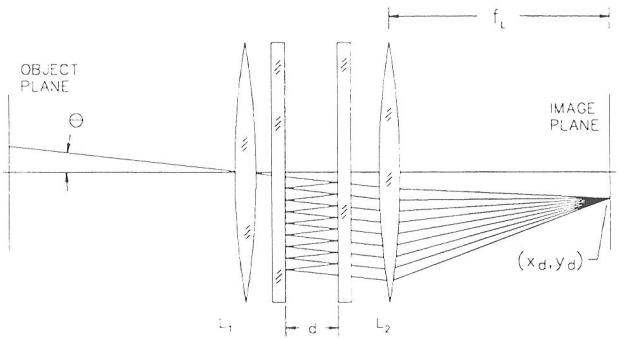

Figure 2.—Fabry-Perot interferometer.

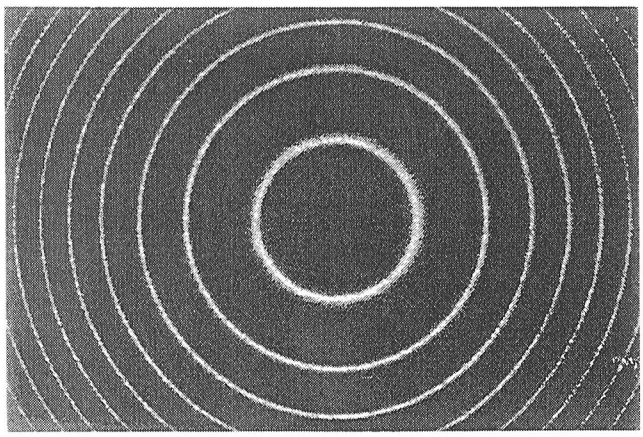

Figure 3.—Fabry-Perot interference fringes.

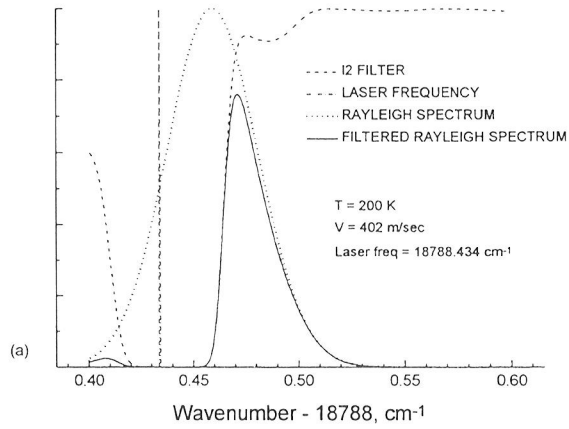

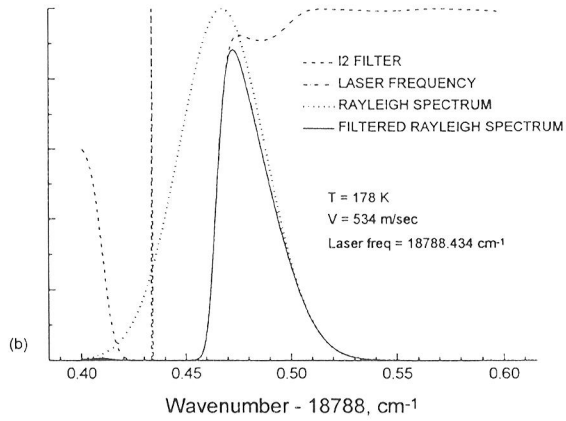

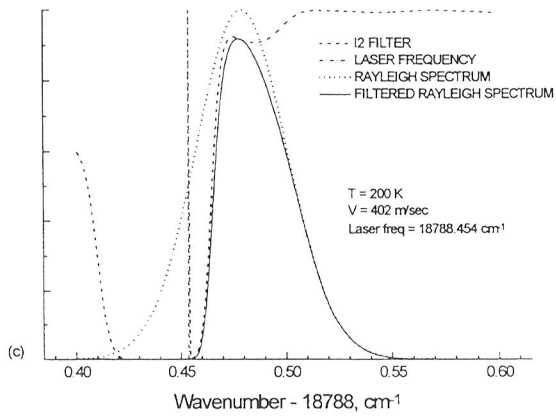

Figure 4.—Filtered Rayleigh scattering spectrum for two flow conditions showing similar spectra (a) and (b) for the laser frequency equal 18788.434 cm^{-1}; the same flow condition as (a) is shown in (c) for a laser frequency of 18788.454 cm^{-1}.

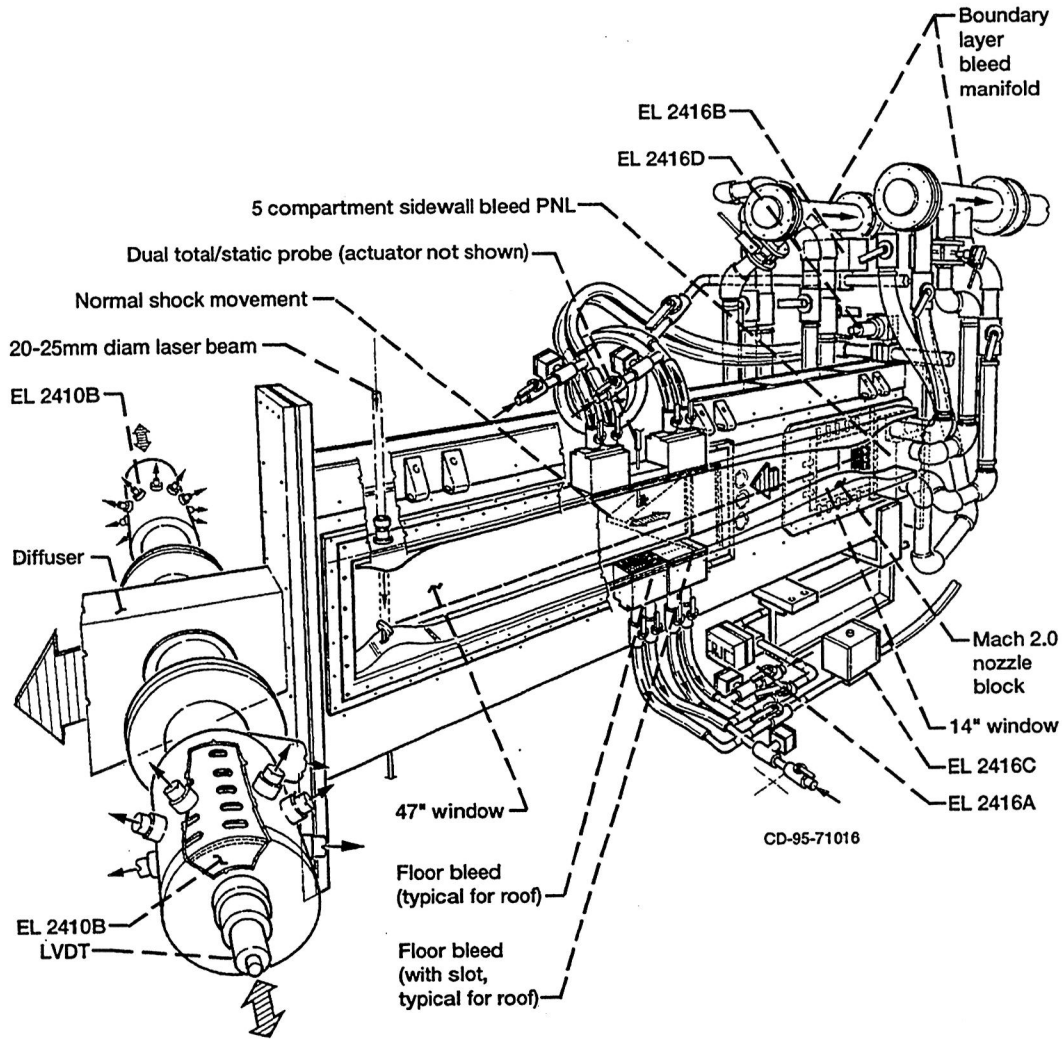

Figure 5.—Supersonic Wind Tunnel (SWT) with shock shape position controls.

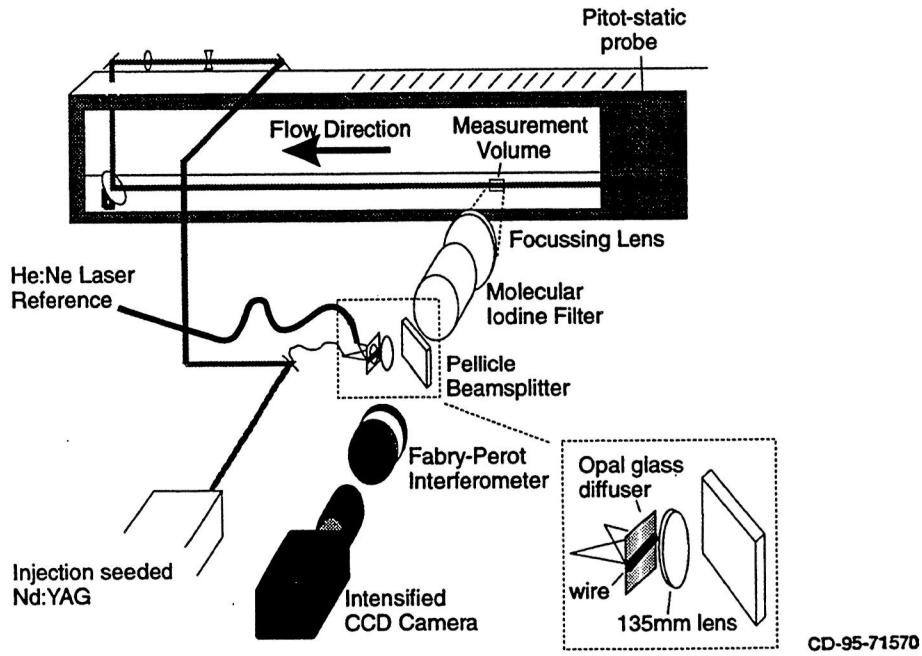

Figure 6.—Optical arrangement for the Rayleigh scattering measurements.

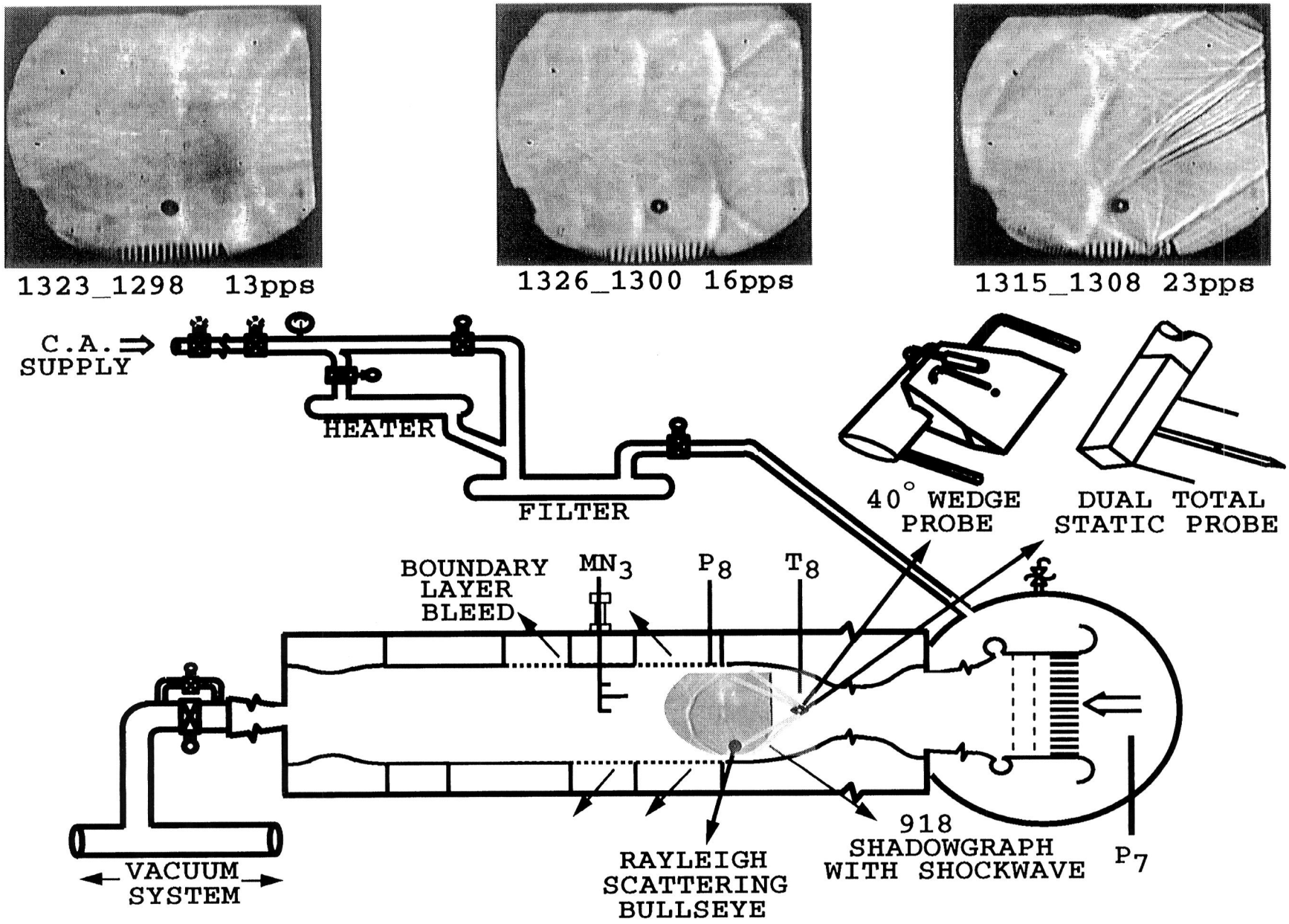

Figure 7.—Probe effects at Mach 2.0 with increasing mass flow.

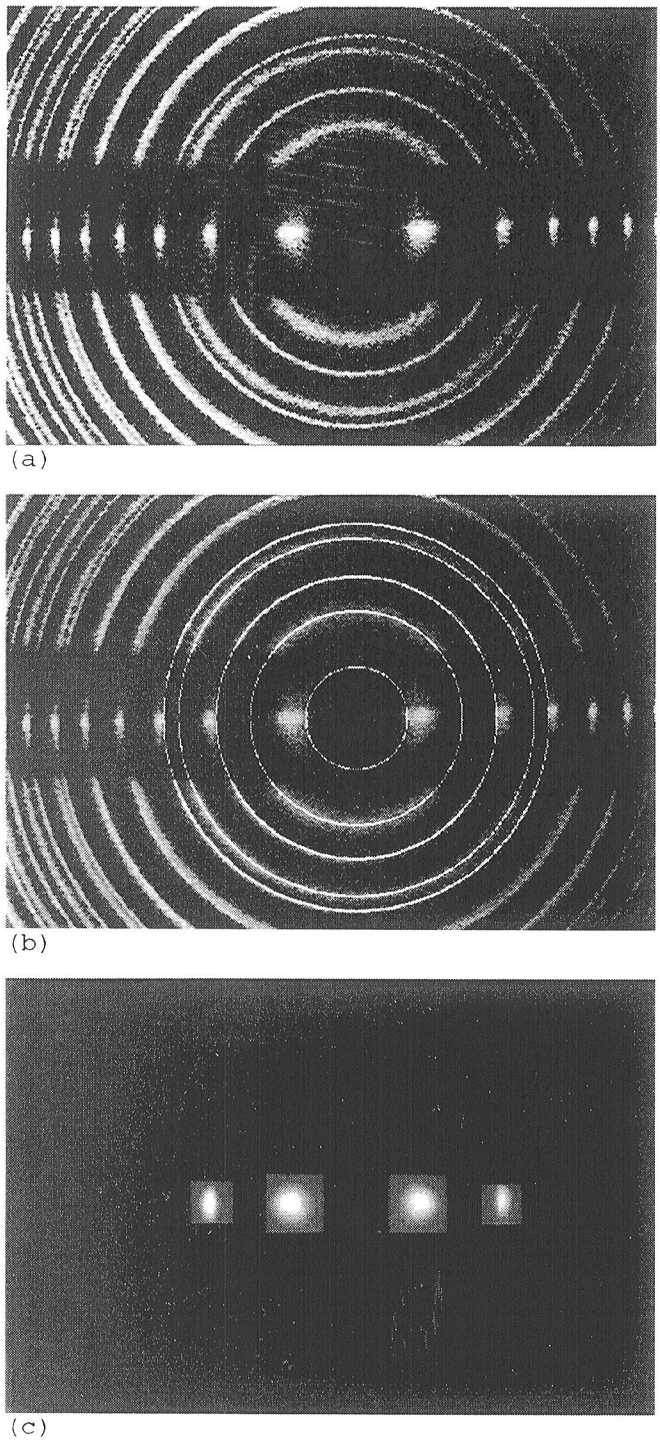

Figure 8.—(a) Image showing Nd:YAG and HeNe reference fringes in upper and lower parts with Rayleigh scattered light in center; (b) image showing fit to Nd:YAG and HeNe reference fringes; (c) fit to model function for four subregions.

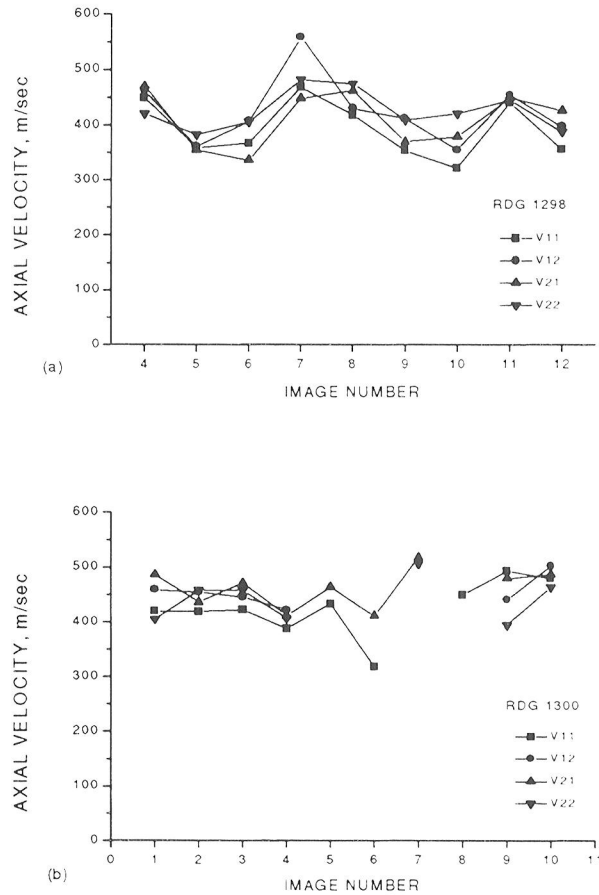

Figure 9.—Axial velocity for number of images for two flow condition: (a) RDG 1298 (b) RDG 1300. Each image is from single laser pulse with velocity determined for four subregions; gaps are result of lack of convergence for certain subregions.

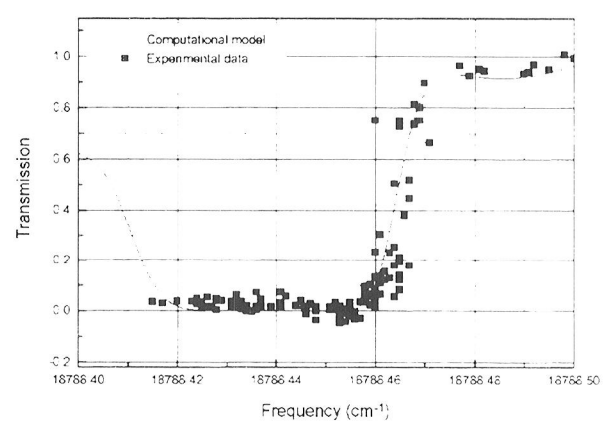

Figure 10.—Transmission of Nd:YAG light through iodine cell.

REPORT DOCUMENTATION PAGE

Form Approved
OMB No. 0704-0188

1. AGENCY USE ONLY (*Leave blank*)	2. REPORT DATE	3. REPORT TYPE AND DATES COVERED
	September 1995	Technical Memorandum

4. TITLE AND SUBTITLE
Instantaneous Flow Measurements in a Supersonic Wind Tunnel Using Spectrally Resolved Rayleigh Scattering

5. FUNDING NUMBERS
WU-505-62-50

6. AUTHOR(S)
Richard G. Seasholtz, Alvin E. Buggele, and Mark F. Reeder

7. PERFORMING ORGANIZATION NAME(S) AND ADDRESS(ES)
National Aeronautics and Space Administration
Lewis Research Center
Cleveland, Ohio 44135-3191

8. PERFORMING ORGANIZATION REPORT NUMBER
E-9870

9. SPONSORING/MONITORING AGENCY NAME(S) AND ADDRESS(ES)
National Aeronautics and Space Administration
Washington, D.C. 20546-0001

10. SPONSORING/MONITORING AGENCY REPORT NUMBER
NASA TM-107042

11. SUPPLEMENTARY NOTES
Prepared for the International Symposium on Optical Science, Engineering, and Instrumentation sponsored by the Society of Photo-Optical Instrumentation Engineers, San Diego, California, July 9-14, 1995. Responsible person, Richard G. Seasholtz, organization code 2520, (216) 433-3754.

12a. DISTRIBUTION/AVAILABILITY STATEMENT
Unclassified - Unlimited
Subject Category 35
This publication is available from the NASA Center for Aerospace Information, (301) 621-0390.

12b. DISTRIBUTION CODE

13. ABSTRACT (*Maximum 200 words*)

Results of a feasibility study to apply laser Rayleigh scattering to non-intrusively measure flow properties in a small supersonic wind tunnel are presented. The technique uses an injection seeded, frequency doubled Nd:YAG laser tuned to an absorption band of iodine. The molecular Rayleigh scattered light is filtered with an iodine cell to block light at the laser frequency. The Doppler-shifted Rayleigh scattered light that passes through the iodine cell is analyzed with a planar mirror Fabry-Perot interferometer used in a static imaging mode. An intensified CCD camera is used to record the images. The images are analyzed at several subregions, where the flow velocity is determined. Each image is obtained with a single laser pulse, giving instantaneous measurements.

14. SUBJECT TERMS	15. NUMBER OF PAGES
Rayleigh scattering; Fabry-Perot interferometers	16
	16. PRICE CODE: A03

17. SECURITY CLASSIFICATION OF REPORT	18. SECURITY CLASSIFICATION OF THIS PAGE	19. SECURITY CLASSIFICATION OF ABSTRACT	20. LIMITATION OF ABSTRACT
Unclassified	Unclassified	Unclassified	

National Aeronautics and
Space Administration
Lewis Research Center
21000 Brookpark Rd.
Cleveland, OH 44135-3191